Struct Chem
DOI 10.1007/s11224-012-0112-1

ORIGINAL RESEARCH

Synthesis, molecular structure, and spectral analyses of ethyl-4-[(2,4-dinitrophenyl)-hydrazonomethyl]-3,5-dimethyl-1*H*-pyrrole-2-carboxylate

R. N. Singh · Amit Kumar · R. K. Tiwari ·
Poonam Rawat · Rajiv Manohar

Received: 26 February 2012 / Accepted: 13 August 2012

Abstract Ethyl-4-[(2,4-dinitrophenyl)-hydrazonomethyl]-3,5-dimethyl-1*H*-pyrrole-2-carboxylate (**3**) has been newly synthesized by the condensation of ethyl-4-formyl-3,5-dimethyl-1*H*-pyrrole-2-carboxylate and 2,4-dinitrophenylhydrazine, characterized by FT-IR, ^{1}H NMR, UV–Vis, DART Mass and elemental analysis. The formation of compound (**3**) and its properties have been evaluated by quantum chemical calculations. The calculated thermodynamic parameters show that the formation reaction of (**3**) is exothermic and spontaneous at room temperature. The vibrational analysis indicates that (**3**) forms dimer in the solid state by heteronuclear double hydrogen bonding (N–H···O). Topological parameters electron density (ρ_{BCP}), Laplacian of electron density ($\nabla^2\rho_{\mathrm{BCP}}$), and total electron energy density (H_{BCP}) at bond critical points (BCP) have been analyzed using "atoms in molecules" (AIM) theory. The interaction energies of dimer formation using DFT and AIM calculations are found to be −14.6509 and −15.5308 kcal/mol, respectively. AIM ellipticity analysis confirms the presence of resonance-assisted hydrogen bonding in dimer. The global electrophilicity index ($\omega = 5.91$ eV) shows that title molecule is a strong electrophile. The local reactivity descriptors Fukui functions (f_k^+, f_k^-), softness (s_k^+, s_k^-), and electrophilicity indices (ω_k^+, ω_k^-) analyses are performed to determine the reactive sites within molecule.

Keywords Density functional theory · Vibrational spectra · Hydrogen bonded dimer · AIM calculation · Reactivity descriptors · Ellipticity

Introduction

The carboxaldehydes of pyrrole form important class of precursors for synthesis of hydrazones and their derivatives. Pyrrole fragment is a constituent of many biological systems. The pyrrole-α-carboxaldehyde has been used for the development of potential chemosensors [1]. Hydrazones are an important class of compounds due to their various properties and applications. They are used as antimicrobial, antitubercular [2–6], and antidiabetic agents [7]. They have strong coordinating ability toward different metal ions [8, 9]. In addition, aroyl hydrazones and their mode of chelation with transition metal ions present in the living system have been of significant interest [10, 11]. The chemical stability of hydrazones and their high melting points have recently made them attractive as prospective new material for opto-electronic applications [1]. The nitrophenyl hydrazones exhibit a series of good organic nonlinear optical (NLO) properties [12–15]. Hydrazones having frame –C$\underline{\mathrm{H}}$=N–NH– constitute an important class of compounds for [2+2] cycloadditions and 1,3 dipolar cycloadditions and have been turned into a valuable tool for the synthesis of azetidinones and pyrazoles, respectively [16, 17] and various other N, O, or S containing heterocyclic compounds such as oxadiazolines, thiazolidinones, triazolines [18–24]. The ethyl-4-formyl-3,5-dimethyl-1*H*-pyrrole-2-carboxylate is a suitable precursor for the

---

Electronic supplementary material The online version of this article (doi:10.1007/s11224-012-0112-1) contains supplementary material, which is available to authorized users.

R. N. Singh (✉) · A. Kumar · R. K. Tiwari · P. Rawat
Department of Chemistry, University of Lucknow, University Road, Lucknow 226007, India
e-mail: rnsvk.chemistry@gmail.com

R. Manohar
Department of Physics, University of Lucknow, University Road, Lucknow 226007, India

synthesis of hydrazones; however, its derivative with 2,4-dinitrophenylhydrazine has not been reported. In this article, we report the synthesis, characterization, and molecular dimer structure of ethyl-4-[(2,4-dinitrophenyl)-hydrazonomethyl]-3,5-dimethyl-1*H*-pyrrole-2-carboxylate (**3**). Experimental work is accompanied by quantum chemical calculations providing information on chemical reactivity and several other properties of the title compound.

Experimental section

Procedures and synthesis of ethyl-4-[(2,4-dinitrophenyl)-hydrazonomethyl]-3,5-dimethyl-1*H*-pyrrole-2-carboxylate (**3**)

Analytical grade 2,4-dinitrophenylhydrazine was purchased from s.d. fine. The solvent methanol was dried and distilled before use according to the standard procedure [25]. Ethyl-4-formyl-3,5-dimethyl-1*H*-pyrrole-2-carboxylate was prepared by an earlier reported method [26]. A solution of 2,4-dinitrophenyl hydrazine (0.1015 g, 0.5125 mmol) in 15 ml methanol was added dropwise with stirring in solution of 20 ml methanol. Reaction mixture was stirred at room temperature for 24 h. After 24 h stirring, precipitate of brown color was appeared. The precipitate was filtered off, washed with methanol, and dried in air. Percentage yield: 20.81. Compound decomposes above 268 °C without melting. The elemental analysis was carried out using Elemental Analyser Vario EL-III. Analysis for $C_{16}H_{17}N_5O_6$: Found C 49.92, H 4.63, N 18.91 %, Calculated C 51.18, H 4.56, N 18.66 %. The ^{1}H NMR spectrum was recorded in DMSO-d_6 on Bruker DRX-300 spectrometer using TMS as an internal reference. The UV–Vis absorption spectrum (1×10^7 M in DMSO) was recorded on ELICO SL-164 spectrophotometer. The FT-IR spectrum was recorded in KBr medium on a Bruker spectrometer. The DART-Mass spectrum was recorded on JMS-T100LC, Accu TOF mass spectrometer. DART Mass: Calc. 375.1178, Found *m*/*z* 375.13 [M^+].

Computational methods

The theoretical calculations for the synthesized compound were carried out with Gaussian 03 program package [27] to predict the molecular structure, ^{1}H NMR chemical shifts, and vibrational wavenumbers using density functional theory (DFT), B3LYP functional and 6-31G(d,p) basis set. B3LYP invokes Becke's three parameters (local, non local, Hartree–Fock) hybrid exchange functional (B3) [28] with Lee–Yang–Parr correlation functional (LYP) [29]. The basis set 6-31G(d,p) with "d" polarization functions on heavy atoms and "p" polarization functions on hydrogen atoms are used for better description of polar bonds of nitro group [30, 31]. It should be emphasized that "p" polarization functions on hydrogen atoms are used for reproducing the out of plane vibrations involving hydrogen atoms. Convergence criterion in which both the maximum force and displacement are smaller than the cutoff values of 0.000450 and 0.001800 and r.m.s. force and displacement are less than the cut-off values of 0.000300 and 0.001200 are used in the calculations. The absence of imaginary frequency verified that stationary points correspond to minima of the potential energy surfaces. The time-dependent density functional theory (TD-DFT) is carried out to find the electronic transitions. The optimized geometrical parameters are used in the calculation of vibrational wavenumbers to characterize all stationary points as minima and their harmonic vibrational wavenumbers are positive. All molecular structures are visualized using software Chemcraft [32] and Gauss-View [33]. Potential energy distribution (PED) along internal coordinates is calculated by Gar2ped software [34]. Internal coordinate system recommended by Pulay et al. [35] is used for the assignment of vibrational modes. To estimate the enthalpy and Gibbs free energy values, thermal corrections to enthalpy and Gibbs free energy calculated at B3LYP/6-31G(d,p) level were added to the calculated total energies. The wave function file generated at B3LYP/6-31G(d,p) basis set from the optimized coordinate was used to calculate the topological parameters by AIM 2000 1.0 software [36]. The atoms in molecules (AIM) method gives the opportunity to have an insight into a region of a system. The theory of AIM efficiently describes H-bonding and its concept without border. One of the advantages of the AIM theory is that one can obtain information on changes in the electron density distribution as result of either bond formation or complexes formation. With respect to change of both the method used and the basis set the reliability and stability of values of AIM parameters have been studied and found that they were almost independent of basis set in case of used functional B3LYP in DFT [37].

Results and discussions

Thermodynamic properties

For the simplicity reactants ethyl-3,5-dimethyl-4-formyl-1*H*-pyrrole-2-carboxylate, 2,4-dinitrophenylhydrazine, product (**3**), and water (byproduct) are abbreviated as 1, 2, 3, and 4, respectively. The calculated enthalpy (*H*), Gibbs free energy (*G*), and entropy (*S*) of 1, 2, 3, 4 and reaction at room temperature are listed in Table 1. The enthalpy change of reaction ($\Delta H_{\text{reaction}}$), Gibbs free energy change

Table 1 Calculated enthalpy (H), Gibbs free energy (G), and entropy (S) of reactants (**1**, **2**), products (**3**, **4**) and reaction at room temperature, using B3LYP/6-31G(d,p)

Parameters	**1**	**2**	**3**	**4**	Reaction
H (a.u.)	−669.126528	−751.78676	−1344.524162	−76.394588	−0.005462
G (a.u.)	−669.185894	−751.838537	−1344.611253	−76.416024	−0.002846
S (cal/mol K)	124.946	108.974	183.298	45.116	−5.506

Table 2 Enthalpy (H), Gibbs free energy (H), entropy (H), their change and equilibrium constant of conversion from monomer to dimer

Thermodynamic parameters	H (a.u.)	G (a.u.)	S (cal/mol K)	ΔH (kcal/mol)	ΔG (kcal/mol)	ΔS (cal/mol K)	K_{eq}
2× Monomer	−2,689.048324	−2,689.222506	366.596	−13.01140	−1.54681	−38.45	13.60
Dimer	−2,689.069059	−2,689.224971	328.146				

of reaction ($\Delta G_{\text{reaction}}$), and entropy change of reaction ($\Delta S_{\text{reaction}}$) are calculated from thermodynamic parameters of reactants and products at room temperature. For overall reaction the enthalpy change of reaction ($\Delta H_{\text{reaction}}$), Gibbs free energy change of reaction ($\Delta G_{\text{reaction}}$), and entropy change of reaction ($\Delta S_{\text{reaction}}$) are found to be −3.4275, −1.7859 kcal/mol and −5.506 cal/mol K, respectively. The calculated negative values for $\Delta H_{\text{reaction}}$ and $\Delta G_{\text{reaction}}$ show that reaction is exothermic and spontaneous at room temperature. Thermodynamic relation between equilibrium constant (K_{T}) and Gibbs free energy change of reaction ($\Delta G_{\text{reaction}}$) at temperature ($T$) is given as

$$K_{\text{T}} = e^{-\Delta G/RT}$$

The value of equilibrium constant (K_{T}) determines the nature of reaction (i) if $K_{\text{T}} > 1$, reaction is favored in forward direction, (ii) if $K_{\text{T}} = 0$, reaction is in equilibrium state, (iii) if $K_{\text{T}} < 1$, reaction is favored in backward direction. Using above equation, equilibrium constant (K_{T}) for title reaction is calculated as 20.37 at room temperature. Therefore, reaction is favored in forward direction at room temperature. This confirms the formation of product (**3**) at room temperature.

The binding energy of dimer is calculated as −14.6509 kcal/mol using DFT calculation. The calculated hydrogen binding energy of dimer formation has been corrected for the basis set superposition error (BSSE) via the standard counterpoise method [38] and found to be −10.5485 kcal/mol. The calculated changes in thermodynamic quantities during the dimer formation in gaseous phase have the negative values of ΔH (kcal/mol), ΔG (kcal/mol), and ΔS (cal/mol K) and incorporated in Table 2, indicating that the dimer formation is exothermic and spontaneous. The calculated equilibrium constant between monomer and dimer is quite high ($K = 13.60$) indicating that dimer formation is highly preferred and as a result even *anti* conformer gets converted to *syn* and finally forms the dimer.

Molecular geometry

Geometry of all the reactants and products involved in chemical reaction were computed at B3LYP/6-31G(d,p) level. The calculated ground state *syn*, and *anti* conformers of the product (**3**) have the energy −1,344.88546024 and −1,344.88472880 a.u., respectively, at room temperature. They have energy difference 0.4589 kcal/mol and exist in ratio 68.6, 31.4 %, respectively, at room temperature. The difference of dihedral angle τ(C3C2C9O12, 178.9051) between *syn* (179.99925°) and *anti* (0.0125°) conformers brings carbonyl oxygen (O12) closer to hydrogen (H33) of *β*-methyl of pyrrole in *anti* conformer, and the consequences are repulsion between atom O12 and H33, increase of the angle C2C9O12 (126.0704°), decrease in hardness, and overall higher in energy. In case of the *syn* conformer, the angle C2C9O12 (122.2857°) is less than *anti* resulting to stabilization of the *syn* conformer. Furthermore, the *syn* conformer has geometrical suitability for intermolecular hydrogen bonding by having pyrrolic NH and ester CO on same side and their role lie in molecular association resulting into dimer. The asymmetry of the N1–C2 and N1–C5 bonds can be explained by electron withdrawing character of the ethoxycarbonyl group and conjugation of the N1–C5 with C4–C3–C2 skeleton. It leads to the elongation of N1–C2 bond. These effects are not only seen in quantum calculation but also reflect in crystal structure of the ethyl-3,5-dimethyl-1*H*-pyrrole-2-carboxylate [39], methyl 4-*p*-tolyl-1*H*-pyrrole-2-carboxylate [40]. The N=O bonds in N22-nitro group are more unsymmetrical due to the formation of intramolecular hydrogen bond (N11–H36···O23). This is not only observed in our theoretical study but also reported in crystal structure of hydrazones [41]. Optimized geometry of dimer is shown in Fig. 1, with atom numbering. Selected optimized geometrical parameters of molecular dimer of (**3**) are listed in Table TS1 in Supplementary material. In dimer, heteronuclear intermolecular hydrogen bonding (N–H···O) between pyrrolic

Fig. 1 The molecular structure of dimer for *syn*-conformer of (**3**) using B3LYP/6-31G(d,p)

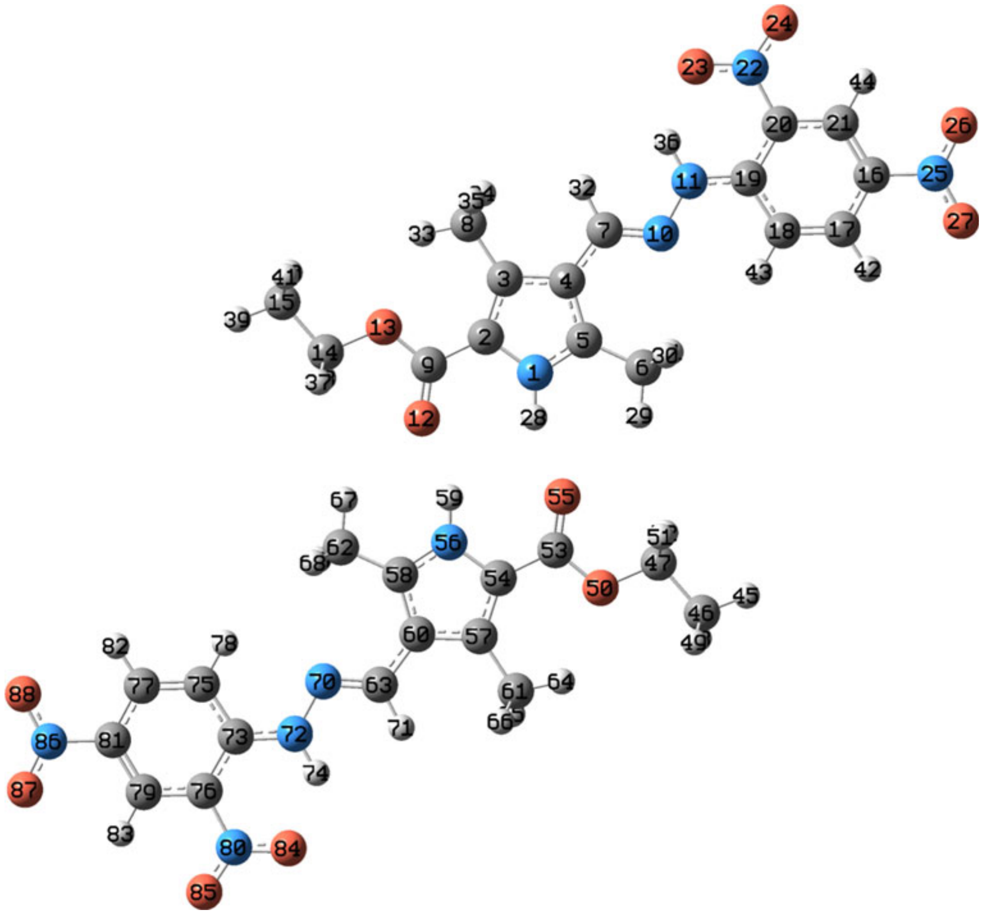

(N–H) and carbonyl (C=O) oxygen of ester form two hydrogen bonds. In intermolecular hydrogen bonds, the N–H bond acts as proton donor and C=O bond as proton acceptor. According to the Etter terminology [42], the cyclic ester dimer form the ten member pseudo ring denoted as $R_2^2(10)$ or more extended sixteen member pseudo ring $R_2^2(16)$ consisting of atoms O12, C9, C2, C3, C4, C5, N1, C55, C53, C54, C57, C60, C58, N56. The superscript designates the number of acceptor centers and the subscript the number of donors in the motif. In dimer, due to intermolecular hydrogen-bond formation both proton donor (N–H bond) and proton acceptor (C=O bond) are elongated from 1.0111 to 1.0207 Å, 1.2230 to 1.2321 Å, respectively. Total energy of the monomer (*syn*-conformer) and its dimer are calculated as −1,344.88546024, −2,689.79426826 a.u., respectively.

^{1}H NMR spectroscopy

The geometry of the title compound, together with that of tetramethylsilane (TMS) is fully optimized. ^{1}H NMR chemical shifts are calculated with GIAO approach using B3LYP functional and 6-31G(d,p) basis set [43]. Chemical shift of any proton is the difference between isotropic magnetic shielding

Table 3 Experimental and calculated GIAO ^{1}H NMR chemical shifts of (**3**) using B3LYP/6-31G(d,p) in DMSO-d_6 as the solvent (25 °C)

Atom no.	δ calc. (ppm)	δ exp. (ppm)	Assignment
H28	9.2597	11.513	(s, 1H, pyrrole-NH)
H29	2.3092	2.475	(s, 3H, pyrrole-CH_3)
H30	2.6527		
H31	2.6524		
H32	8.0748	8.758	(s, 1H, CH=N)
H33	3.0491	2.409	(s, 3H, pyrrole-CH_3)
H34	2.1274		
H35	2.1272		
H36	11.9065	11.798	(s, 1H, hydrazide –NH)
H37	4.3239	4.200–4.271	(q, 2H, CH_2 ester)
H38	4.3217		
H39	1.2095	1.281–1.327	(t, 3H, CH_3 ester)
H40	1.4739		
H41	1.4741		
H42	8.5518	7.793–8.346	(m, 2H, Ar–H)
H43	7.8691		
H44	9.3416	8.845	(s, 1H, Ar–H)

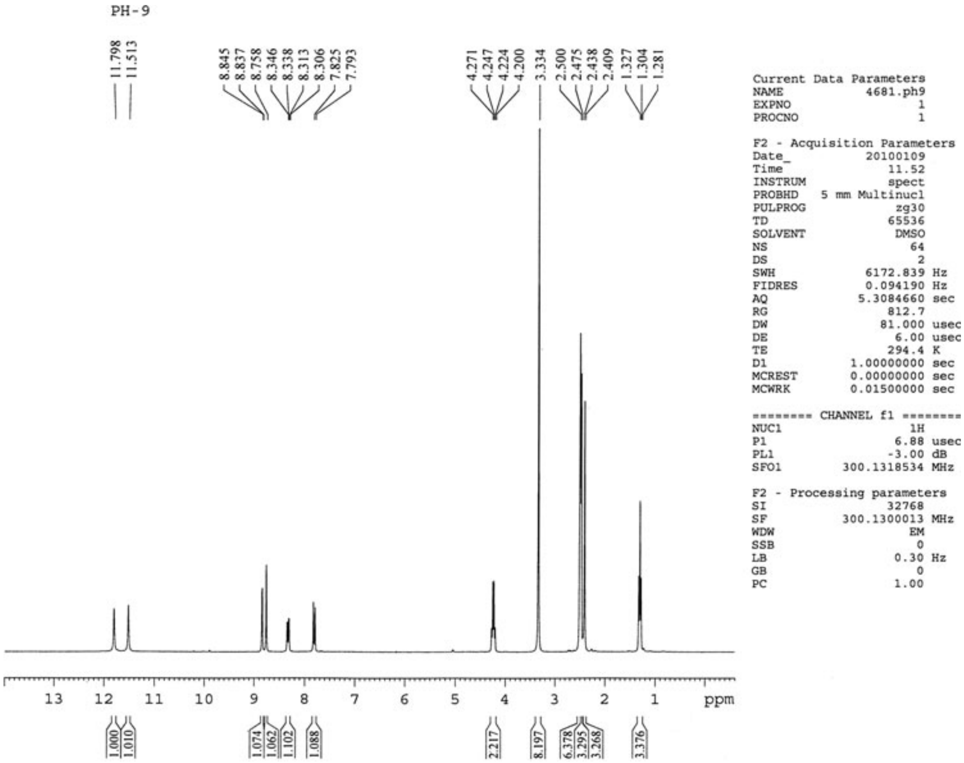

```
Current Data Parameters
NAME             4681.ph9
EXPNO                   1
PROCNO                  1

F2 - Acquisition Parameters
Date_            20100109
Time                11.52
INSTRUM             spect
PROBHD   5 mm Multinucl
PULPROG              zg30
TD                  65536
SOLVENT              DMSO
NS                     64
DS                      2
SWH              6172.839 Hz
FIDRES           0.094190 Hz
AQ              5.3084660 sec
RG                  812.7
DW                 81.000 usec
DE                   6.00 usec
TE                  294.4 K
D1             1.00000000 sec
MCREST         0.00000000 sec
MCWRK          0.01500000 sec

======== CHANNEL f1 ========
NUC1                   1H
P1                   6.88 usec
PL1                 -3.00 dB
SFO1          300.1318534 MHz

F2 - Processing parameters
SI                  32768
SF            300.1300013 MHz
WDW                    EM
SSB                     0
LB                   0.30 Hz
GB                      0
PC                   1.00
```

Fig. 2 The experimental ^{1}H NMR spectrum of (**3**)

(IMS) of TMS and that proton. Experimental and calculated ^{1}H NMR chemical shifts of the title compound are listed in Table 3. The experimental ^{1}H NMR chemical shifts are shown in Fig. 2. To compare the chemical shifts correlation graph between the experimental and calculated chemical shifts was drawn. The correlation graph follows the linear equation ($y = 1.05505x - 0.13678$), where y is the experimental ^{1}H NMR chemical shift, x is the calculated ^{1}H NMR chemical shift. The high value of correlation coefficient ($R^2 = 0.9613$) shows that a good agreement exist between experimental and calculated chemical shifts. The hydrogen experience more deshielding effect when hydrogen bonding is strong and less deshielded when hydrogen bonding is diminished. Thus, the presence of the intramolecular hydrogen bond N11–H35···O23 is supported by the ^{1}H NMR spectrum where the signal of N11–H35 proton appeared with the high value of chemical shift at 11.798 ppm.

UV–Vis spectroscopy

The nature of the transitions observed in the UV–Vis spectrum of (**3**) has been studied by the TD-DFT. The values of calculated electronic transitions of high oscillatory strength and observed are listed in Table TS2 in Supplementary material. The both absorption graph experimental and theoretical UV–Vis spectrum are shown in Fig. 3a. Selected molecular orbital plots involved in electronic excitations are shown in Fig. 3b. The theoretical spectrum of (**3**) is given in Fig. 1 in Supplementary material. The FMOs are important in determining the ability of a molecule to absorb light and molecular reactivity. The vicinal orbitals of HOMO and LUMO play the role of electron donor and electron acceptor, respectively. The $\lambda_{\max}$ is a function of substitution, the stronger the acceptor character of the substituents, the more electron withdraw from the ring, the shorter the $\lambda_{\max}$. From the charge transfer viewpoint, the high value of $|\varepsilon_{\mathrm{HOMO}}|$ means that the ionization is more difficult, that is to say, that molecule is hard to lose electron. The HOMO–LUMO energy gap is an important stability index. The HOMO–LUMO energy gap of title molecule reflects the chemical stability of the molecule.

$$\text{HOMO energy} = -5.8613\,\text{eV}$$

$$\text{LUMO energy} = -2.7355\,\text{eV}$$

$$\text{HOMO-LUMO energy gap} = 3.1258\,\text{eV}$$

TD-DFT calculations using B3LYP/6-31G(d,p) predict three intense electronic transitions at $\lambda_{\max} = 240$ nm, $f = 0.4021$; $\lambda_{\max} = 303$ nm, $f = 0.3958$ and $\lambda_{\max} = 439.49$ nm, $f = 0.7145$. The calculated electronic transitions at $\lambda_{\max} = 240$, 303, and 439 nm are in agreement with the experimental electronic transitions observed at $\lambda_{\max}$ 251, 293, and 401 nm, respectively. The calculated values for wavelength of maximum absorption ($\lambda_{\max}$) are also in agreement with the reported $\lambda_{\max}$ in literature [44]. According to the TD-DFT calculations, the experimental bands at 251, 293, and 401 nm originate mainly due to the

Fig. 3 **a** UV–Vis spectra (experimental and theoretical) for (**3**). ▶ **b** Selected molecular orbital plots involved in electronic excitations for (**3**)

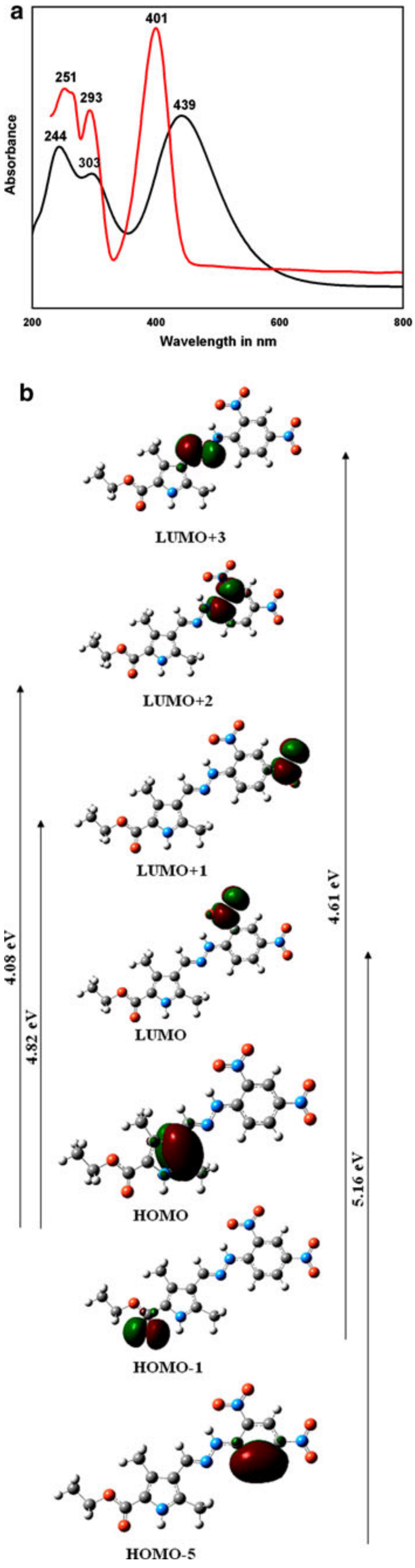

Homo−1 → Lumo+4, Homo → Lumo+3 and Homo → Lumo+2 excitations, respectively. Figure 4b predicts that Homo and Lomo+2 orbitals are localized over pyrrole ring and benzene ring, respectively. Homo → Lumo+3 are localized over C2–C3C8–C4 of pyrrole ring and N25–O26 of nitro group, respectively. The theoretical transition at 293 nm arises due to transition Homo → Lumo+3. The Homo-5 orbital are localized over the benzene ring and Lumo over the nitro group. On the basis of molecular orbital coefficients analyses and molecular plots, these electronic excitations show $\pi \rightarrow \pi^*$, $\pi \rightarrow \pi^*$, and $n \rightarrow \pi^*$ transition, respectively.

Vibrational spectroscopy

The experimental and theoretical (selected) vibrational wavenumbers of dimer at B3LYP/6-31G(d,p) level and their assignments using PED are given in Table 4. The calculated (monomer, dimer) and the experimental FT-IR spectra of (**3**) in the region 4,000–400 cm^{-1} are shown graphically in Fig. 4a, b. The total number of atoms in monomer and dimer are 44 and 88 which give 126 and 258, $(3n - 6)$ vibrational modes for monomer and dimer, respectively. The calculated vibrational wavenumbers have higher values than their experimental for the majority of the normal modes. Two factors may be responsible for the discrepancies between the experimental and computed wavenumbers of this compound. The first is caused by difference of the environment (gas and solid phase) and the second is due to the fact that the experimental values are anharmonic wavenumbers while the calculated values are harmonic ones. Therefore, calculated wavenumbers at B3LYP/6-31G(d,p) level are scaled down using single scaling factor 0.9608 [45], to discard the anharmonicity present in real system. The observed wavenumbers are in good agreement with the calculated wavenumbers of dimer than monomer. Therefore, observed wavenumbers are assigned using dimer PED.

N–H vibrations

The elongation of N–H bond and red shift of corresponding band positions are observed in the dimer, as compared to the monomer. In the experimental FT-IR spectrum of (**3**), the N–H stretch of pyrrole (ν_{NH}) is observed at 3,290 cm^{-1}, whereas it is calculated as 3,334 cm^{-1} in dimer and 3,496 cm^{-1} in monomer. The observed wavenumber at 3,290 cm^{-1} is in good agreement with the calculated wavenumber of dimer. The observed value of ν_{NH} also correlates with the earlier reported strong absorption at

3,358 cm^{-1} for hydrogen bonded pyrrole-2-carboxylic acid dimer recorded in KBr pellet, but it deviates to the reported free ν_{NH} band at higher wavenumber 3,465 cm^{-1}, recorded in CCl_4 solution [46]. Therefore, solid state spectrum of (**3**) attributes to the vibration of hydrogen bonded N–H group. The observed N–H wagging mode of pyrrole at 796 cm^{-1} is calculated at same wavenumber in theoretical IR-spectrum. The observed N–H deformation of pyrrole at 1,563 cm^{-1} agrees well with the calculated wavenumber at 1,544 cm^{-1}.

C–H vibrations

Three methyl groups are present in the molecule. They are abbreviated as Me, Me1, and Me2. Me1 and Me2 are directly attached to the C5 and C3 carbon of pyrrole ring. Me is attached to the CH_2 of ester group. The observed C–H stretching vibrations of benzene ring, ester methyl, and Schiff C–H at 3101, 2983, and 2930 cm^{-1} are in agreement with the calculated wavenumber at 3139, 3018, and 2945 cm^{-1}, respectively. A combination band of CH_2 wagging and pyrrole N–H deformation observed at 1,282 cm^{-1} agrees well with the calculated wavenumber at 1,271 cm^{-1}. The observed rocking mode of Me at 1,022 cm^{-1} corresponds to the calculated wavenumber at 1,088 cm^{-1}. Asymmetric deformation of Me1 observed at 1,420 cm^{-1} agrees well with the calculated wavenumber at 1,412 cm^{-1}.

C–O vibrations

The stretching mode of carbonyl group ($\nu_{C=O}$) is observed at 1,679 cm^{-1}, whereas it is calculated as 1,656 cm^{-1} in dimer and 1,693 cm^{-1} in monomer. The observed $\nu_{C=O}$ agrees well with the earlier reported wavenumber at 1,665 cm^{-1} for dimer of *syn*-pyrrole-2-carboxylic acid [46]. The observed $\nu_{C=O}$ absorption band at 1,679 cm^{-1} is also in good agreement with the calculated wavenumber of dimer. Therefore, $\nu_{C=O}$ stretching mode in (**3**) confirms the involvement of C=O group in intermolecular hydrogen bonding. The observed C9–O13 stretching mode at 1,141 cm^{-1} corresponds to the calculated wavenumber at 1,176 cm^{-1} with 8 % contribution in dimer PED.

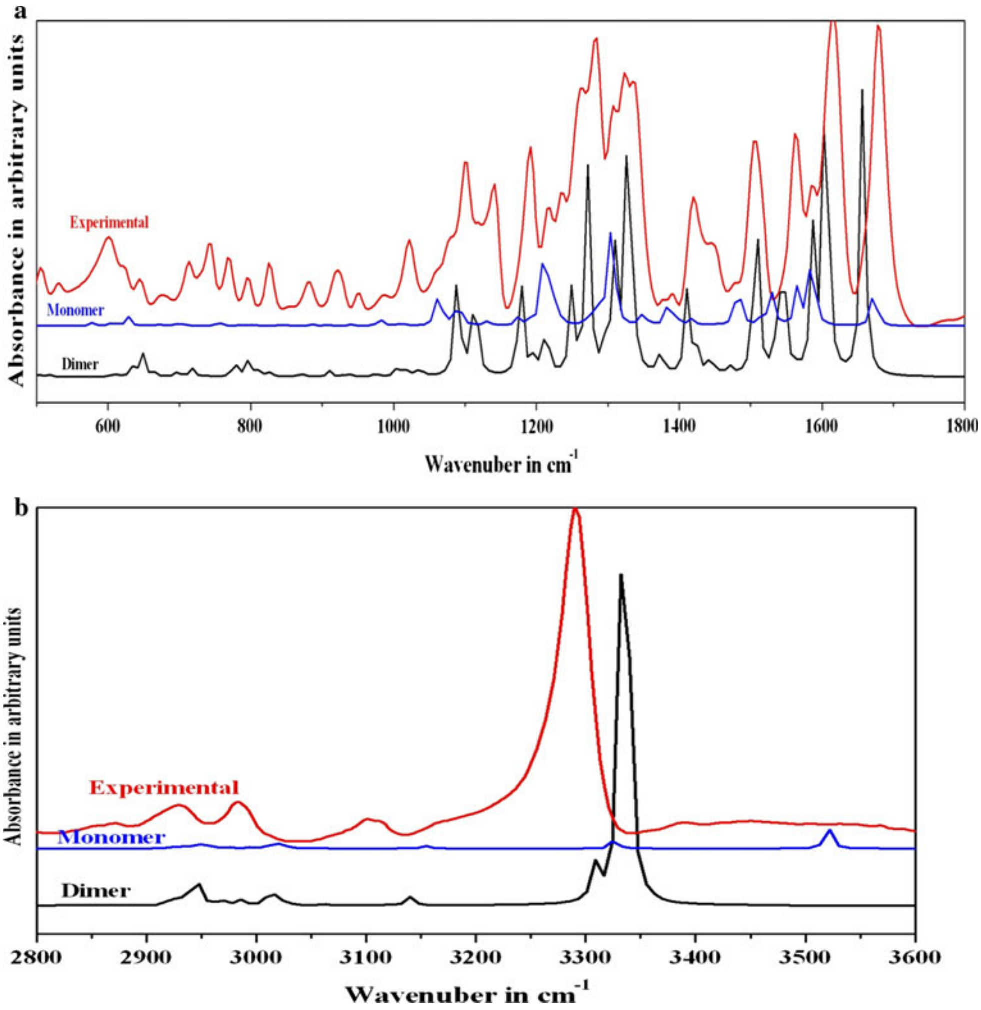

Fig. 4 **a** FT-IR spectra (experimental and calculated) for (**3**) in the region 500–1,800 cm^{-1}. **b** FT-IR spectra (experimental and calculated) for (**3**) in the region 2,800–3,600 cm^{-1}

Table 4 Positions of experimental and theoretical (selected) vibrational bands of dimer using B3LYP/6-31G(d,p) and their assignments [harmonic vibrational wavenumbers (cm^{-1}), IR$_{int}$ (K mmol^{-1})]

Mode no.	Positions of scaled theoretical bands	IR$_{int}$	Exp. bands	Assignment (PED) ≥ 5 %
1	3,334	3,071.47	3,290	ν(N1H28)(52) − ν(N56H59)(48)
2	3,139	49.35	3,101	ν(C79H83)(61) − ν(C21H44)(38)
3	3,018	57.83	2,983	ν(C15H41)(26) − ν(C15H40)(24) − ν(C46H48)(19) ν(C46H49)(18)
4	2,945	74.57	2,930	ν(C7H32)(50) − ν(C63H71)(48)
5	1,656	1,760.65	1,679	ν(C53O55)(33) − ν(C9O12)(33) − ν(C53C54)(5)
6	1,604	1,968.11	1,615	ν(C17C18)(8) − ν(C75C77)(8) + ν(C20C21)(5) − ν(C76C79)(5)
7	1,587	834.89	1,586	ν(N86O88)(11) − ν(N25O27)(11) − ν(N86O87)(11) + ν(N25O26)(11)
8	1,544	912.7	1,563	δ(C54H59N56)(12) − δ(C2H28N1)(12) − ν(C4C5)(8) + ν(C58C60)(8) + ν(C2C3)(7) − ν(C54C57)(7)
9	1,507	1,085.05	1,506	ν(N11C19)(6) − ν(C73N72)(6) + ν(C16C17)(6) − ν(C77C81)(6) − ν(C58N56)(5) + ν(N1C5)(5)
10	1,412	278.06	1,420	(δ_{as}-Me1)(5) − (δ_{as}-Me1)(5)
11	1,327	1,616.4	1,323	ν(N86O88)(8) − ν(N25O27)(8) + ν(N86O87)(6) − ν(N25O26)(6) − ν(C81N86)(5) + ν(C16N25)(5)
12	1,271	1,230.87	1,282	δ(C54H59N56)(12) − δ(C2H28N1)(11) − ν(C9O13)(6) + ν(C53O50)(6) + (ω-C14H37H38)(5) − (ω-C47H51H52)(5) − ν(C53C54)(5) + ν(C2C9)(5)
13	1,250	531.37	1,235	ν(N80O84)(10) − ν(N22O24)(10) − δ(C76H83C79)(6) − δ(C16H44C21)(6) − δ(C81H82C77)(5) + δ(C16H42C17)(5) − (ρ-N72C74)(5) − (ρ-N11H36)(5) − ν(C76N80)(5) + ν(C20N22)(5)
14	1,213	330.25	1,217	ν(N1C2)(12) − ν(C54N56)(11) − ν(C5C6)(6) + ν(C58C62)(5) + ν(C5C6)(5) − ν(C60C63)(5)
15	1,197	119.2	1,191	δ(C73H78C75)(11) + δ(C17H43C18)(11) − δ(C76H83C79)(7) − δ(C16H44C21)(7) + (ρ-N72C74)(6) + (ρ-N11H36)(6)
16	1,176	657.52	1,141	ν(C53O50)(8) − ν(C54N56)(8) − ν(C9O13)(8) + ν(N1C2)(8) − δ(C54H59N56)(7) + δ(C2H28N1)(7)
17	1,113	511.73	1,101	δ(C81H82C77)(18) − δ(C16H42C17)(17) + δ(C73H78C75)(9) + δ(C17H43C18)(9)
18	1,088	609.56	1,022	ν(N10N11)(7) − ν(N70N72)(7)
19	1,036	54.29	951	(τ-C9C2)(16) + (τ-C53C54)(12) − (τ-R)(6) − δ(C16H44C21)(5) − (τ-R)(5)
20	1,004	68.42	921	ν(C14C15)(20) − ν(O13C14)(16) − ν(C46C47)(12) − (τ-C9C2)(10) + ν(C47H51)(9)
21	908	39.36	881	ν(C81N86)(7) − ν(C16N25)(7) − ν(C76N80)(6) − ($\delta_{trigonal}$-R1)(6) ν(C20N22)(6) − ($\delta_{trigonal}$-R1)(6)
22	796	116.07	796	(ω-N56H59)(24) + (ω-N1H28)(24) − (τ-O12H59)(22) − (τ-O55H28)(21)
23	777	93.82	769	(τ-C9C2)(10) + (τ-C53C54)(10) + (ω-C2C9)(6) + (ω-C53C54)(6)
24	716	44.74	713	(ω-C53C54)22) + (τ-C53C54)(22) + (ω-C2C9)(19) + (τ-C9C2)(19)
25	647	156.85	644	(τ-R)(16) − (τ-C58C62)(15) + (τ-R)(14) − (τ-C5C6)(14) − (τ-C53C54)(10) − (τ-C9C2)(9) + (ω-C58C62)(5)
26	607	11.52	600	(ω-C2C9)(14) + (ω-C53C54)14) − (τ-R)(8) − (τ-R)(7) + (τ-C5C6)(6) + (τ-H67O12)(6) + (τ-H29O55)(6) + (τ-C58C62)(6)
27	515	17.11	506	(ρ-C16N25)(25) + δ(O87C81N86)(22) + δ(C77N86C81)(5) − δ(C17N25C16)(5)

Proposed assignment and PED for vibrational modes: types of vibrations: ν—stretching, ρ—rocking (in-plane vibration), ω—wagging (out of plane vibration), δ—deformation, δ_{as}—asymmetric deformation, τ—torsion. R—pyrrole ring, R1—benzene ring

N=O vibrations

The molecule under investigation possesses two nitro groups. The nitro groups show two type of stretching vibrations as asymmetric and symmetric. Asymmetric stretching vibrations are always observed at higher wavenumber than symmetric stretching vibrations. The observed asymmetric stretching vibrations of nitro group ($\nu_{N=O}$) at

1,586 cm^{-1} agrees well with the calculated wavenumber at 1,587 cm^{-1}. Symmetric stretching vibration of $\nu_{\mathrm{N=O}}$ is observed at 1235, 1323 cm^{-1}, whereas it is calculated as 1250, 1327 cm^{-1}, respectively. The observed wavenumbers are in agreement with the earlier reported wavenumbers for asymmetric and symmetric vibration of nitro group at 1,600 and 1,319 cm^{-1}, respectively [47].

C–N and C–C vibrations

The observed C19–N11 stretching vibration at 1,506 cm^{-1} agrees well with the calculated wavenumber at 1,507 cm^{-1}. The observed C16–N25 rocking mode at 881 cm^{-1} corresponds to the calculated wavenumber at 908 cm^{-1}. The observed C–C stretches in benzene ring at 1,615 cm^{-1} corresponds to the calculated wavenumber at 1,604 cm^{-1}, respectively. A combination band of C–C stretching and C2H28N1 deformation in pyrrole ring is observed at 1,563 cm^{-1}, whereas it is calculated as 1,544 cm^{-1}.

AIM calculation

The experimental and computational data show that H-bonding exerts substantial changes on the molecular geometry of the distant parts of the system. These changes are related to the variations in π-electron delocalization and reflect the strength of H-bonding. In both intramolecular and intermolecular H-bonding π-electron delocalization effects are detectable and characterized with the use of the QTAIM methods. There are several interacting effects such as dynamic disorder, orientational disorder, and mesomeric effect connected with hydrogen bonding especially in crystal structures. Geometrical as well as topological parameters are useful tool to characterize the strength of hydrogen bond. The geometrical criteria for the existence of hydrogen bond are as follows: (i) The distance between proton (H) and acceptor (A) to be less than the sum of their van der Waal's radii of these atoms, (ii) the "donor (D)–proton (H)···acceptor (A)" angle to be >90°, (iii) the elongation of "donor (D)–proton(H)" bond length to be observed. These criteria are frequently considered as insufficient; therefore, the existence of hydrogen bond could be supported further by Koch and Popelier criteria [48] based on "AIM" theory (i) The existence of bond critical point for the "proton (H)···acceptor (A)" contact, (ii) the value of electron density ($\rho_{\mathrm{H\ldots A}}$) should be within the range 0.002–0.040 a.u., (iii) the corresponding Laplacian ($\nabla^2\rho_{\mathrm{BCP}}$) should be within the range 0.024–0.139 a.u. According to Rozas et al. [48], the H-bonding may be classified as (i) Strong H-bonds: having ($\nabla^2\rho_{\mathrm{BCP}}$) < 0 and $H_{\mathrm{BCP}} < 0$, covalent in nature, (ii) medium H-bonds: having ($\nabla^2\rho_{\mathrm{BCP}}$) > 0 and $H_{\mathrm{BCP}} < 0$, partially covalent in nature, (iii) weak H-bonds: having ($\nabla^2\rho_{\mathrm{BCP}}$) > 0 and $H_{\mathrm{BCP}} > 0$, mainly electrostatic in nature and the distance between interacting atoms is greater than the sum of van der Waal's radii of these atoms.

Molecular graph of the dimer using AIM program at B3LYP/6-31G(d,p) level is shown in Fig. 5. According to these parameters, there exist three types of interactions as (i) O23···H36, O84···H74 are medium hydrogen bonds, (ii) O12···H59, O55···H28 are weak hydrogen bonds, (iii) O50···H64, O13···H33, O12···H67, O55···H29, C6···N10, C62···N70 are weak interactions. AIM topological (density and energetic) parameters of various interactions of molecular complex are tabulated in Table TS3 in Supplementary material. Espinosa [49] proposed proportionality between hydrogen bond energy (E) and potential energy density (V_{BCP}) at H···O contact: $E = ½\ (V_{\mathrm{BCP}})$. The intermolecular interaction energy of dimer formation as per DFT calculation found to be -14.6509 kcal/mol and after BSSE correction is -10.5485 kcal/mol and as per AIM calculations is -15.5307 kcal/mol, respectively. The heteronuclear intramolecular N–H···O hydrogen bond energy is calculated as -9.4035 kcal/mol using AIM calculations.

The strength of H-bonds in dimer is often resulting of the existence of dynamic disorder, orientational disorder, and mesomeric effect but may also be explained within the conditions related to the resonance-assisted H-bonding (RSHB). In dimer, often there is equalization of certain bonds, potential double movement of protons between electronegativity atoms of electron excess. In RAHBs model, there is an effective mixing in two forms. The ellipticity (ε) at bond critical points (BCP) is a sensitive index to monitor the π-character of bond. The ε is related to λ_1 and λ_2, which correspond to the eigen values of Hessian and defined as by a relationship: $\varepsilon = (\lambda_1/\lambda_2) - 1$. To investigate the effect of π-electron delocalization in bonds associated with N and O atoms of N–H···O heteronuclear inter and intramolecular hydrogen bonds, the analysis of the bond ellipticity is performed. In dimer, inter and intramolecular hydrogen bonds are associated with the sixteen member and six member pseudo rings, respectively. These rings are abbreviated as Ring1 and Ring2, respectively. The ε values for bonds involved in Ring1 and Ring2 are given in Table TS4 in Supplementary material. In Ring1, the values of ε for bonds O12–C9, C9–C2, C2–C3, C3–C4, C4–C5, C5–N1 associated with the N1–H28···O55 and for bonds O55–C53, C53–C54, C54–C57, C57–C60, C60–C58, C58–N56 associated with the N56–H59···O12 are in the range 0.1005–0.2904. In Ring2, the values of ε for bonds N11–C19, C19–C20, C20–N22, N22–O23 associated with the N11–H36···O23 are in the range 0.1131–0.2301. These values of ε correspond to the aromatic bonds reported in literature [50]. The ε values confirm the presence of resonance-assisted intermolecular and intramolecular hydrogen bonds because

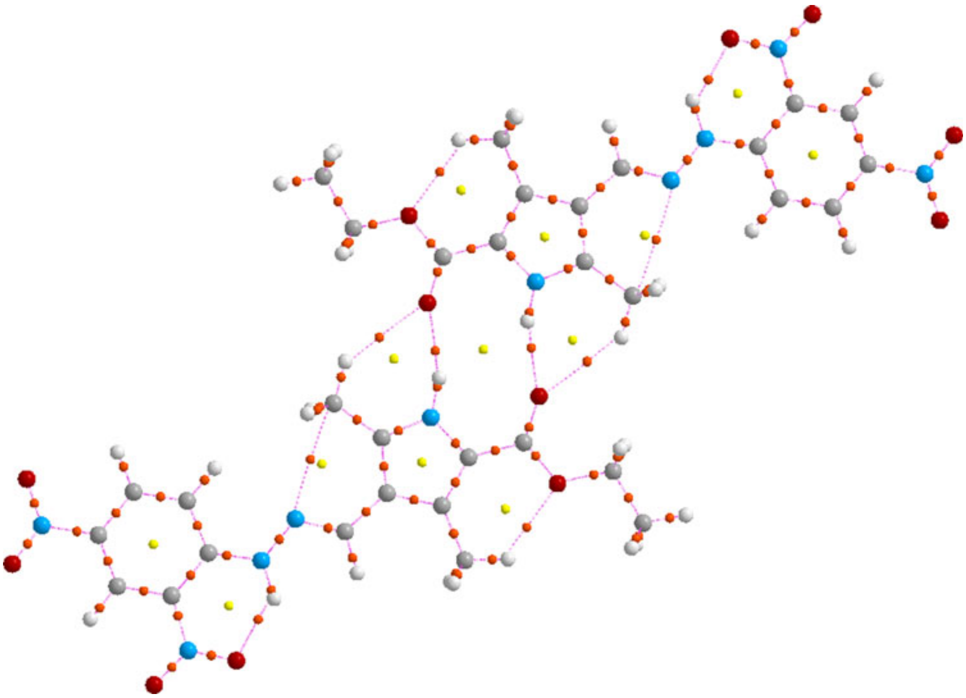

Fig. 5 Molecular graph of (**3**) dimer: bond critical points (*small red spheres*), ring critical points (*small yellow sphere*), bond paths (*pink lines*) (Color figure online)

both N and O atoms are interconnected by a system of π-conjugated double bonds.

Chemical reactivity

Global reactivity descriptors

On the basis of Koopman's theorem [51], global reactivity descriptors electronegativity (χ), chemical potential (μ), global hardness (η), global softness (S), and global electrophilicity index (ω) are calculated using the energies of frontier molecular orbitals $\varepsilon_{\mathrm{HOMO}}$, $\varepsilon_{\mathrm{LUMO}}$ and given by Eqs. (1–5) [51–55]:

$$\chi = 1/2(\varepsilon_{\mathrm{LUMO}} + \varepsilon_{\mathrm{HOMO}}) \tag{1}$$

$$\mu = \chi = 1/2(\varepsilon_{\mathrm{LUMO}} + \varepsilon_{\mathrm{HOMO}}) \tag{2}$$

$$\eta = 1/2(\varepsilon_{\mathrm{LUMO}} - \varepsilon_{\mathrm{HOMO}}) \tag{3}$$

$$S = 1/2\eta \tag{4}$$

$$\omega = \mu^2/2\eta \tag{5}$$

Electrophilicity index (ω) measures the stabilization in energy when the system acquires an additional electronic charge (ΔN_{max}) from the environment. The energies of frontier molecular orbitals ($\varepsilon_{\mathrm{HOMO}}$, $\varepsilon_{\mathrm{LUMO}}$), energy gap ($\varepsilon_{\mathrm{LUMO}} - \varepsilon_{\mathrm{HOMO}}$), electronegativity ($\chi$), chemical potential ($\mu$), global hardness ($\eta$), global softness ($S$), and global electrophilicity index (ω) for reactants **1**, **2**, and product (**3**) are listed in Table TS5 in Supplementary material. The calculated high value of (ω) for (**3**) shows that the title molecule to be a strong electrophile than reactants 1 and 2.

Local reactivity descriptors

Fukui functions ($f_{\mathrm{k}}^{+}, f_{\mathrm{k}}^{-}, f_{\mathrm{k}}^{0}$), local softnesses ($s_{\mathrm{k}}^{+}$, s_{k}^{-}, s_{k}^{0}), and local electrophilicity indices (ω_{k}^{+}, ω_{k}^{-}, ω_{k}^{0}) have been described earlier in literature [54, 55]. Using Hirshfeld population analyses of neutral, cation and anion state of molecule, Fukui Functions are calculated at same calculation method B3LYP/6-31G(d,p) using Eqs. (7–9):

$$f_{\mathrm{k}}^{+} = [q(N+1) - q(N)] \quad \text{for nucleophilic attack} \tag{7}$$

$$f_{\mathrm{k}} = [q(N) - q(N-1)] \quad \text{for electrophilic attack} \tag{8}$$

$$f_{\mathrm{k}}^{0} = 1/2[q(N+1) + q(N-1)] \quad \text{for radical attack,} \tag{9}$$

where N, $N-1$, $N+1$ are total electrons present in neutral, cation, and anion state of molecule, respectively.

Local softnesses and electrophilicity indices are calculated using the following equations (10, 11).

$$s_{\mathrm{k}}^{+} = Sf_{\mathrm{k}}^{+},\ s_{\mathrm{k}}^{-} = Sf_{\mathrm{k}}^{-},\ s_{\mathrm{k}}^{0} = Sf_{\mathrm{k}}^{0} \tag{10}$$

$$\omega_{\mathrm{k}}^{+} = \omega f_{\mathrm{k}}^{+},\ \omega_{\mathrm{k}} = \omega f_{\mathrm{k}}^{-},\ \omega_{\mathrm{k}}^{0} = \omega f_{\mathrm{k}}^{0}, \tag{11}$$

where +, −, 0 signs show nucleophilic, electrophilic, and radical attack respectively.

Fukui functions ($f_{\mathrm{k}}^{+}, f_{\mathrm{k}}^{-}$), local softnesses ($s_{\mathrm{k}}^{+}$, s_{k}^{-}), local electrophilicity indices (ω_{k}^{+}, ω_{k}^{-}) for selected atomic sites of (**3**) are listed in Tables TS6 and TS7 in Supplementary material, using Mulliken and Hirshfeld population analyses, respectively. The maximum values of all the three local electrophilic reactivity descriptors (f_{k}^{+}, s_{k}^{+}, ω_{k}^{+}) at C(7) indicate that this site is more prone to nucleophilic attack. The calculated local reactivity descriptors of synthesized molecule (**3**) favor the formation of new heterocyclic compounds such as azetidinones, oxadiazolines, and thiazolidinones etc. by attack of nucleophilic part of the dipolar reagent on the C(7) site and electrophilic part of dipolar reagent on the N(10) site of C7=N10 bond.

Conclusions

In this study, title compound (**3**) has been synthesized and characterized by ^{1}H NMR, UV–Vis, FT-IR spectroscopy, and elemental analysis. Experimental and theoretical ^{1}H NMR chemical shifts are in good agreement to each other. Experimental electronic absorption spectra have some blue shifts compared with theoretical data and molecular orbital coefficients analyses suggest that electronic transitions are to $\pi \rightarrow \pi^*$ and $n \rightarrow \pi^*$type. The experimental vibrational wavenumbers agree well with the calculated wavenumbers of dimer, supporting the existence of dimer in the solid state. The energy strength for intra and intermolecular hydrogen bonds are calculated as −9.4035, −6.1226 kcal/mol, respectively. The energy values confirm the medium nature of intra and intermolecular hydrogen. AIM ellipticity analyses confirm the presence of resonance-assisted intra and intermolecular hydrogen bonds in dimer. In addition, theoretical results from reactivity descriptors are in complete agreement with observed reactivity of such type of compounds. The local electronic reactivity descriptors show that azomethine carbon (C7) is more reactive site for nucleophilic attack and may be used as precursor for the syntheses of new heterocyclic compounds such as azetidinones, oxadiazolines, and thiazolidinones.

Acknowledgments The authors are thankful to the DST New Delhi for financial supports.

References

1. Yu M, Lin H, Lin H (2007) Ind J Chem Sect A 46:1437
2. Rauf A, Banday MR, Mattoo RH (2008) Acta Chim Slov 55:448
3. Rollas S, Gülerman N, Erdeniz H (2002) Farmaco 57:171
4. Kozminykh VO, Belyaev AO, Kozminykh Bukanova EV, Odegova TF (2004) J Pharma Chem 38:368
5. Zheng LW, Wu LL, Zhao BX, Dong WL, Miao JY (2009) Bioorg Med Chem 17:1957
6. Sriram D, Yogeeswari P, Devakaram RV (2006) Bioorg Med Chem 14:3113
7. Smalley TL Jr, Peat AJ, Boucheron JA, Dickerson S, Garrido D, Preugschat F, Schweiker SL, Thomson SA, Wang TY (2006) Bioorg Med Chem 16:2091
8. Raman N, Ravichandran S, Thangaraja C (2004) J Chem Sci 116:215
9. Jasinski JP, Guild CJ, Kumar CSC, Yathirajan HS, Mayekar AN (2010) Bull Korean Chem Soc 31:881
10. Lalib L, Mohamed LA, Iskander MF (2002) Transit Met Chem 25:700
11. Affan MA, Foo IPP, Fasihuddin BA, Sim EUH, Hapipah MA (2009) Malays J Anal Sci 13:73
12. Szczesna B, Lipkowska U (2001) Supramol Chem 13:247
13. Vijayakumar S, Adithya A, Sharafudeen KN, Balakrishna K, Chandrasekharan K (2010) J Mod Opt 57:670
14. Vijayakumar S, Adhikari A, Kalluraya B, Sharafudeen KN, Chandrasekharan K (2011) J Appl Polym Sci 119:595
15. Kwon O, Jazbinsek M, Yun H, Seo J, Kim E, Lee Y, Gunter P (2008) Cryst Growth Des 8:4021
16. Deng X, Mani NS (2008) Org Lett 10:1307
17. Deng X, Mani NS (2008) J Org Chem 73:2412
18. Nakayama Y, Sanemitsu Y (1984) J Org Chem 49:1703
19. Dogan HN, Duran A, Rollas S, Sener G, Armutak Y, Uysal MK (1998) Med Sci Res 26:755
20. Küçükgüzel SG, Kocatepe A, De Clercq E, Sahin F, Güllüce M (2006) Eur J Med Chem 41:353
21. Küçükgüzel SG, Oruç EE, Rollas S, Sahin F, Ozbek A (2002) Eur J Med Chem 37:197
22. Korotchenko VN, Shastin AV, Nenaidenko VG, Balenkova ES (2003) Russ J Org Chem 39:527
23. Kaïm LE, Gautier L, Grimaud L, Harwood LM, Michaut V (2003) Green Chem 54:779
24. Kotali A, Lafazanis IS (2003) Arkivoc (vi):91
25. Vogel AI (1956) Practical organic chemistry. Prentice Hall Publication, New York 344
26. Chu EJH, Chu TC (1954) J Org Chem 19:266
27. Frisch MJ, Trucks GW, Schlegel HB, Scuseria GE, Robb MA, Cheeseman JR Jr, Montgomery JA, Vreven T, Kudin KN, Burant JC, Millam JM, Iyengar SS, Tomasi J, Barone V, Mennucci B, Cossi M, Scalmani G, Rega N, Petersson GA, Nakatsuji H, Hada M, Ehara M, Toyota K, Fukuda R, Hasegawa J, Ishida M, Nakajima T, Honda Y, Kitao O, Nakai H, Klene M, Li X, Knox JE, Hratchian HP, Cross JB, Bakken V, Adamo C, Jaramillo J, Gomperts R, Stratmann RE, Yazyev O, Austin AJ, Cammi R, Pomelli C, Ochterski JW, Ayala PY, Voth K, Morokuma GA, Salvador P, Dannenberg JJ, Zakrzewski VG, Dapprich S, Daniels AD, Strain MC, Farkas O, Malick DK, Rabuck AD, Raghavachari K, Foresman JB, Ortiz JV, Cui Q, Baboul AG, Clifford S, Cioslowski J, Stefanov BB, Liu G, Liashenko A, Piskorz P, Komaromi I, Martin RL, Fox DJ, Keith T, Al-Laham MA, Peng CY, Nanayakkara A, Challacombe M, Gill PMW, Johnson B, Chen W, Wong Wong MW, Gonzalez C, Pople JA (2004) Gaussian 03, Revision C.02. Gaussian, Inc., Wallingford, CT
28. Becke AD (1993) J Chem Phys 98:5648
29. Lee CT, Yang WT, Parr RGB (1988) Phys Rev 37:785
30. Petersson DA, Allaham MA (1991) J Chem Phys 94:6081
31. Petersson GA, Bennett A, Tensfeldt TG, Allaham MA, Mantzaris WAJ (1988) J Chem Phys 89:2193
32. Zhurko GA, Zhurko DA (2005) Chemcraft: lite version build 08 (freeware)
33. Computer program Gauss-view 3.09, Ver 2, Gaussian Inc, Pittsburgh, PA
34. Martin JML, Alsenoy V, Alsenoy CV (1995) Gar2ped, University of Antwerp
35. Pulay P, Fogarasi G, Pang F, Boggs JE (1979) J Am Chem Soc 101:2550
36. Bader RFW (1990) Atoms in molecules. A quantum theory. Oxford University Press, Oxford
37. Jablonski M, Palusiak M (2010) J Phys Chem A 114:2240
38. Boys SF, Bernardi F (1970) Mol Phys 19:553–556
39. Arrannja CT, Siva MR, Beja AM, Ferreira AFPV, Sobral AJFN (2008) Acta Cryst E64:o1989
40. Gardiner MG, Jones RC, Ng S, Smith JA (2007) Acta Cryst E63:o470
41. Shan S, Tian YL, Wang SH, Wang WL, Xu YL (2008) Acta Cryst E64:o1153

42. Etter MC (1990) Acc Chem Res 23:120
43. Wolinski K, Hinton JF, Pulay JF (1990) J Am Chem Soc 112:8251
44. Jackuemin D, Perpète EA (2007) J Mol Struct Theochem 804:31
45. Sundaraganesan N, Kavitha E, Sebastian S, Cornard JP, Martel M (2009) Spectrochim Acta Part A 74:788–797
46. Dubis AT, Grabowski SJ, Romanowska DB, Misiaszek T, Leszczynski J (2002) J Phys Chem A 106:10613
47. Sundaraganesan N, Ayyappan S, Umamaheswari H, Joshua BD (2007) Spectrochim Acta Part A 17:17
48. Rozas I, Alkorta I, Elguero J (2000) J Am Chem Soc 122:11154
49. Espinosa E, Molins E, Lecomte C (1998) Chem Phys Lett 285:170
50. Matta IF, Boyd RJ (2007) An introduction to the quantum theory of atoms in molecules. Wiley-VCH Verlag Gmbh, Berlin
51. Parr RG, Yang W (1989) Density functional theory of atoms and molecules. Oxford University Press, Oxford
52. Parr RG, Pearson RG (1983) J Am Chem Soc 105:7512
53. Geerlings P, De Proft F, Langenaeker W (2003) Chem Rev 103:1793
54. Parr RG, Szentpály L, Liu S (1999) J Am Chem Soc 121:1922
55. Chattaraj PK, Giri S (2007) J Phys Chem A 111:11116